ELSEVIER

Journal of Nuclear Materials 318 (2003) 207–214

journal of nuclear materials

www.elsevier.com/locate/jnucmat

Microstructure in martensitic steels T91 and F82H after irradiation in SINQ Target-3

X. Jia, Y. Dai *

Spallation Neutron Source Division, Paul Scherrer Institut 5232, Villigen PSI, Switzerland

Abstract

T91 and F82H martensitic steels were irradiated in the Swiss spallation neutron source Target-3 to a maximum dose of 11.8 dpa in a temperature range of 90–360 °C. Transmission electron microscope observations were performed to study radiation effects on the microstructure at different irradiation doses and temperatures. The results for the unirradiated and irradiated conditions indicate that there is no significant difference between the microstructures of the two steels. High-density helium bubbles of size about 1 nm are observed in samples irradiated at temperatures above about 200 °C to about 10 dpa with 550 appm He. The helium bubbles observed in T91 steel have slightly higher density but smaller size as compared to those in F82H steel at the same irradiation conditions. The density and size of defect clusters in a T91 sample are almost the same as those in a F82H sample at the same dose. In both steels, the size increases while the density drops rapidly with irradiation temperature above about 250 °C. The amorphization of $M_{23}C_6$ precipitates was observed again in T91 and F82 samples irradiated at 220 °C and below.

1. Introduction

Martensitic steels are candidate materials for the containers of liquid targets of the spallation neutron source and accelerator driven systems facilities. In the last few years, a number of studies were carried out to investigate the mechanical properties and microstructure of martensitic stainless steels irradiated with 800 MeV protons [1–5]. However, the irradiation temperatures in all these studies were low, below 230 °C. At temperatures above 200 °C, the irradiation effects produced by high-energy protons and spallation neutrons on the mechanical properties and the microstructure of martensitic steels are little understood. In our previous work the microstructure of F82H steel irradiated in the Swiss spallation neutron source (SINQ) Target-3 in a temperature range of 140–360 °C to doses of 10–12 dpa was studied [6]. It showed that high-density small helium bubbles formed in the samples irradiated at $\geqslant 175$ °C. In this work, three F82H samples of lower doses (2.7, 3.8 and 5.8 dpa) and six T91 samples irradiated up to 11.8 dpa at similar conditions have been studied. This investigation has provided the useful information for interpreting the results of mechanical tests on T91 steel [7].

2. Experimental

T91 steel received from Oak Ridge national laboratory has a composition of 8.32 Cr, 0.86 Mo, 0.48 Mn, 0.20 V, 0.06 Ni, 0.06 Nb and 0.09 C in wt%, and balance Fe. The plate (Heat #30176) was cold-rolled from 6 to 3 mm, and was subjected to a heat treatment: normalized at 1040 °C for 1 h, rapidly cooled then tempered at 760 °C for 1 h. F82H steel (IEA Heat 9741) used in this irradiation has a composition of 7.65 Cr, 2 W, 0.16 Mn, 0.16 V, 0.02 Ta, 0.11 Si and 0.09 C in wt%, and balance Fe. The 15 mm thick plate was subjected to a heat treatment: normalized at 1040 °C for 38 min and tempered at 750 °C for 1 h, to produce a final fully tempered martensite lath structure [8].

* Corresponding author. Tel.: +41-56 310 4171; fax: +41-56 310 4529.

E-mail address: yong.dai@psi.ch (Y. Dai).

0022-3115/03/$ - see front matter © 2003 Elsevier Science B.V. All rights reserved.
doi:10.1016/S0022-3115(03)00101-6

Table 1
Irradiation condition and defect TEM measurement results for T91 and F82H samples

Materials	No.	Irradiation temperature[a] (°C)	dpa	He (appm)[b]	Defect density (m^{-3})	Defect size (nm)	Helium bubble density (m^{-3})	Bubble size (nm)	Amorphization of precipitates
F82H	P13	360	11.8	1115	1.5×10^{22}	8.1	4.3×10^{23}	1.6	No
	P1	295	9.7	670	2.7×10^{22}	6.5	4.0×10^{23}	1.4	No
	P16	255	10.1	735	3.8×10^{22}	5.5	4.2×10^{23}	1.2	No
	RC-01	235	9.9	560	3.6×10^{22}	3.6	4.7×10^{23}	0.9	Yes/no
	RC-02	210	9.9	560	3.4×10^{22}	3.5	4.6×10^{23}	0.8	Yes
	RC-05	175	9.9	560	3.0×10^{22}	3.3	5.1×10^{23}	0.7	Yes
	P17	140	9.4	705	3.6×10^{22}	3.7	–	–	Yes
	P15	200	5.7	375	1.9×10^{22}	3.7	–	–	Yes
	P20	110	3.8	225	2.7×10^{22}	3.2	–	–	Yes
	Pb	90	2.7	145	2.6×10^{22}	2.1	–	–	Yes
T91	I14	360	11.8	1115	1.3×10^{22}	8.9	5.1×10^{23}	1.4	No
	I8	295	10.1	725	3.3×10^{22}	5.4	5.3×10^{23}	1.2	No
	Id	250	8.3	540	3.6×10^{22}	4.5	5.4×10^{23}	1.1	No
	I10	205	5.8	380	1.8×10^{22}	4.4	–	–	Yes
	Ic	130	4.6	235	2.5×10^{22}	3.8	–	–	Yes
	I6	110	3.8	225	2.1×10^{22}	3.0	–	–	Yes

[a] The values of the irradiation temperature in the table are the average values of the irradiation temperatures during the two irradiation periods. The difference of the irradiation temperatures in the two periods is about 15% of the average values.
[b] The He concentration data have been updated with the measurement results [10].

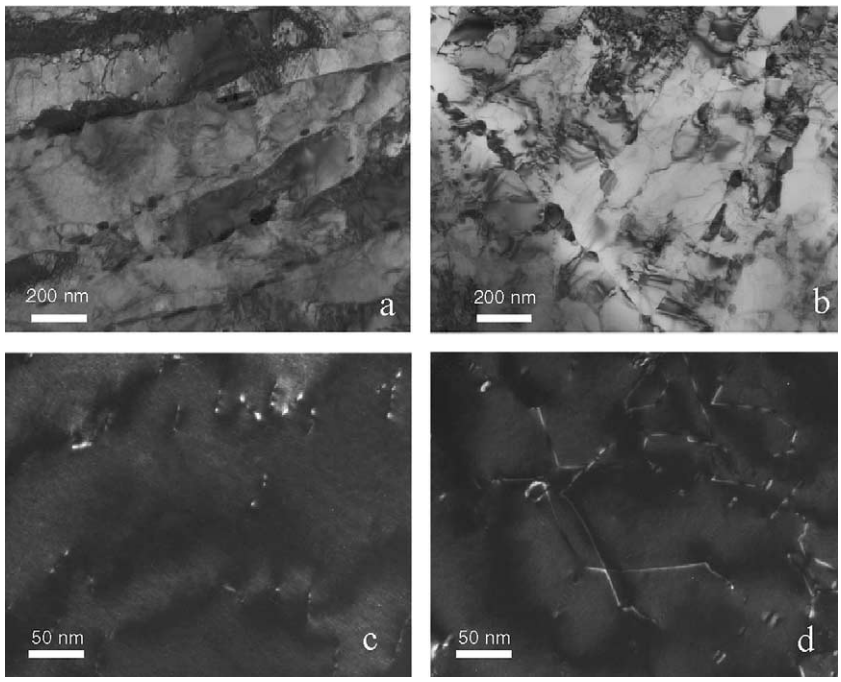

Fig. 1. The microstructure of unirradiated F82H ((a) and (c)) and T91 ((b) and (d)) steels. (a) and (b) BF images showing precipitate and martensite lath structures in F82H and T91, respectively; (c) and (d): WBDF images showing the dislocation structures in F82H and T91, respectively.

Transmission electron microscope (TEM) samples of both materials were irradiated at different positions (Rods 1, 3, 4, 5 and 10) in SINQ Target-3 to get a series of irradiation conditions. The irradiation was performed with a total proton current of about 0.85 mA for the first 12 months and about 1.04 mA for the last 2 months of the real beam time. The difference of the irradiation temperatures in these two periods is as great as 15% of the temperature values as shown in Table 1. The temperature values given in this report are the average values of those in the two periods. The TEM samples used in this study were irradiated in a temperature range of 90–360 °C. The irradiation dose of the samples ranges from 2.7 to 11.8 dpa. The corresponding helium concentration is in between 145 and 1115 appm. More detailed information can be found in Refs. [9,10]. The information of

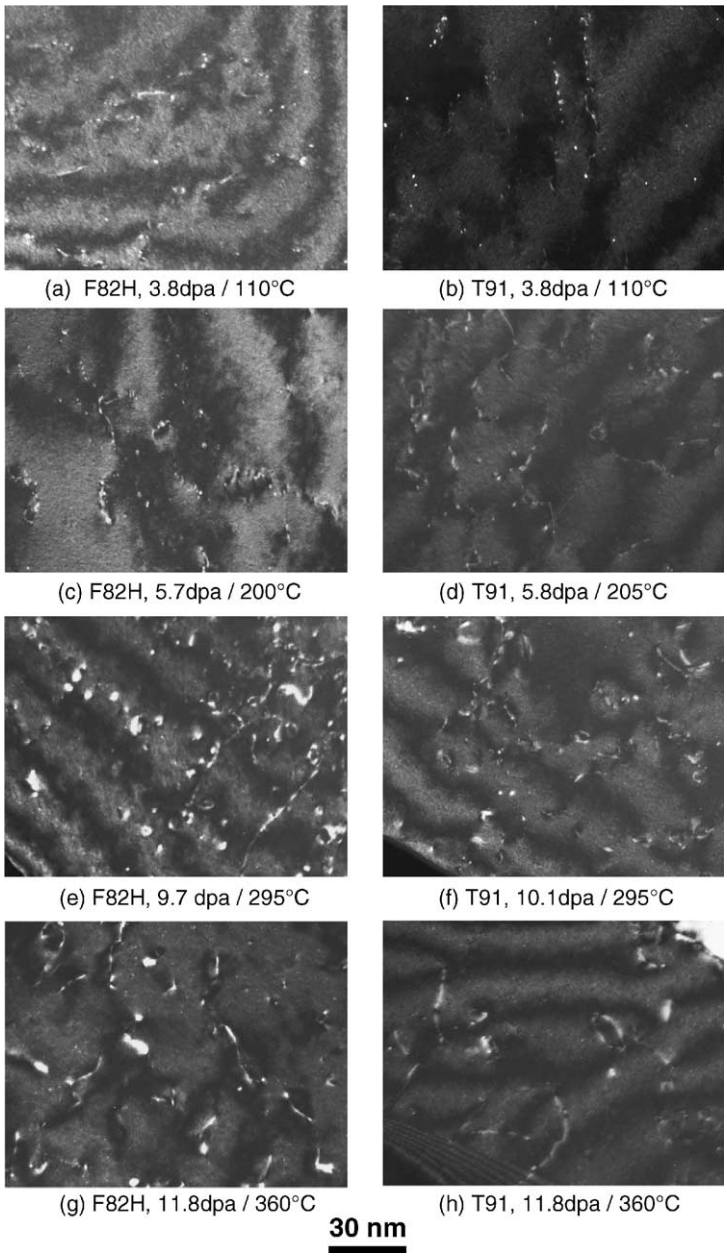

Fig. 2. Defect cluster structure of irradiated F82H (left column) and T91 (right column) samples. The irradiation conditions are indicated below the micrographs. The scale for all the micrographs is the same as indicated at the bottom.

irradiation doses and temperatures of the samples is summarized in Table 1.

In order to reduce the magnetic effect and radioactivity of the samples, the preparation is optimized using 1 mm diameter disk technique [11]. The samples were ground from 250 μm down to 150 μm, then electropolished in a Tenupol-3 using a solution of 5% perchloric acid + 95% methanol at −20 °C and 50 V.

Observations were conducted on a JEOL-2010 TEM operated at 200 kV. The most often used image conditions were bright field (BF) and weak beam dark-field (WBDF) at $\mathbf{g}(4\mathbf{g})$ and $\mathbf{g}(5\mathbf{g})$, $\mathbf{g} = \mathbf{110}$ near $\mathbf{z} = \mathbf{001}$, or $\mathbf{111}$. The Stereo pair technique was also used to investigate the tiny helium bubbles. For all specimens, only the micrographs of $\mathbf{g}(5\mathbf{g})$ $\mathbf{g} = \mathbf{110}$, $\mathbf{z} = \mathbf{111}$ were used for quantifying the size and number density of defect clusters. The thickness for observation of defect clusters was $\leqslant 50$ nm, which was deduced from the number of fringes with an uncertainty of about ±15%. In addition, the real density of defect clusters should be greater than what obtained from the micrographs taken at a single image condition. 2-beam BF micrographs of 250,000 times magnification were used for counting He bubbles.

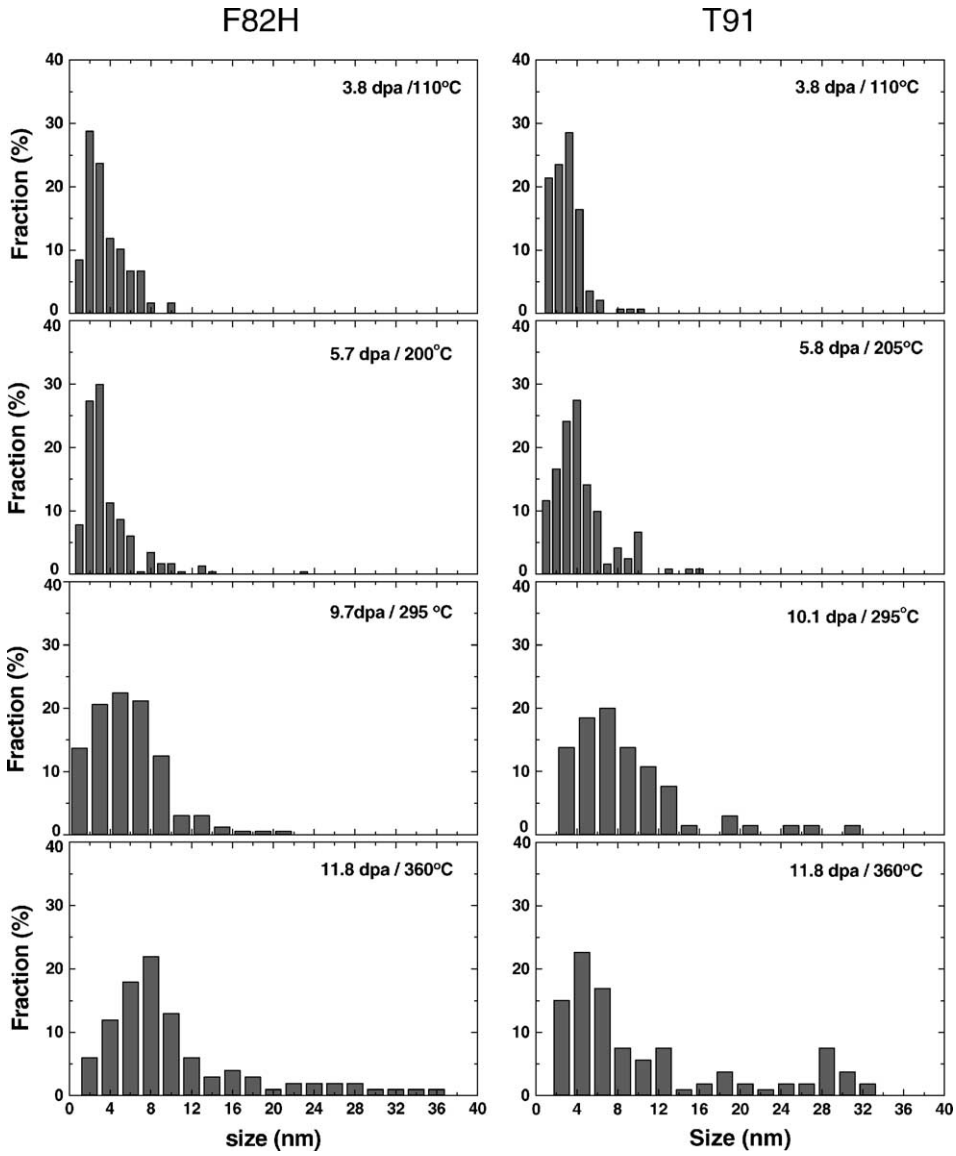

Fig. 3. Defect size distributions for F82H (left column) and T91 (right column) samples at different irradiation conditions.

3. Results and discussion

The microstructures of F82H and T91 steels prior to irradiation are quite similar. Both steels have a typical martensitic lath structure containing dislocations with a density of approximately 1×10^{14} m^{-2}. The dislocation density in T91 steel is slightly higher than in F82H. $M_{23}C_6$ type carbide precipitates were identified mainly along prior austenite grain boundaries and martensite lath boundaries. The size of precipitates varies from few tens nm to ~2 μm, see Fig. 1.

Fig. 2 presents a comparison between the irradiation induced defect structures in F82H and T91 steels. The irradiation introduced significant changes in the microstructure of both materials. Irradiation induced defects, namely defect clusters or dislocation loops, were observed at all the irradiation doses. At low irradiation doses and also low irradiation temperatures, the main feature is small defect cluster, which can be seen in Fig. 2(a) and (b) for both of steels irradiated to 3.8 dpa at 110 °C. With increasing irradiation dose and irradiation temperature, the defect clusters become larger, as shown in Fig. 2(c) and (e) for F82H, Fig. 2(d) and (f) for T91 irradiated to 5.7 dpa at ~200 °C, and to 10.1 dpa at 295 °C, respectively. At the highest dose of 11.8 dpa and the highest irradiation temperature of 360 °C, the loop size is maximum while the density decreases substantially (Fig. 2(g) and (h)). The size distributions of defect clusters for both steels are plotted in Fig. 3. It demonstrates that the size of defect clusters increases with irradiation dose. At the same (or similar) irradiation conditions the size distributions of both steels look very similar. Fig. 4 shows the temperature dependence of the density and the size of defect clusters for F82H and T91 in a dose range of 8.3–11.8 dpa. Although the dose varies a little, it is clear that both the size and density are insensitive to irradiation temperature below about 250 °C. At higher temperature, the size increases while the density drops quickly. In Fig. 5(a) and (b) the size and density of defect clusters are plotted verse irradiation dose, respectively. Since the size and density depend strongly on irradiation temperature above 250 °C, the data of 295 and 360 °C are not included. The results are somewhat different from the linear dose dependence observed in F82H and Optimax irradiated with 800 MeV protons at $\leqslant 60$ °C up to 6 dpa [3]. Fig. 5(a) illustrates that the size of defect clusters increases with dose up to about 6 dpa then turns to saturate. The density data presented in Fig. 5(b) are very scattered. Nevertheless, it can be seen that the density increases significantly from lower doses (2.7–5.8 dpa) to higher doses (8.3–10.1 dpa). It is clear that the data presented in Fig. 5(a) and (b) are very limited to make a definite conclusion. More detailed study is on the way.

The high-density helium bubbles with an average size around 1 nm were observed in F82H steels irradiated in SINQ Target-3 at about 175 °C and above [6]. The stereo pair of WBDF images presented in Fig. 6 shows that the helium bubbles distribute homogeneously in the matrix of the specimen. This is different from that in high temperature helium implanted T91 and EM10 showed by Henry et al. [12], where helium bubbles locate

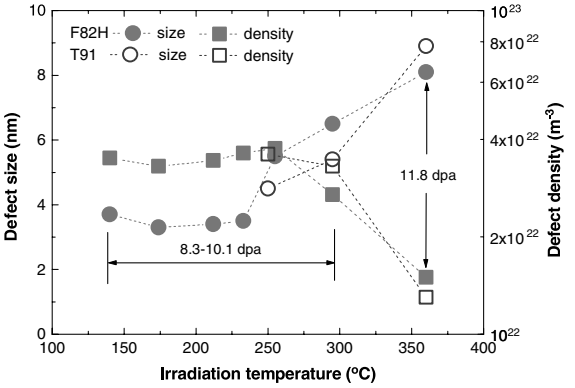

Fig. 4. The temperature dependence of the density and the size of defect clusters for F82H and T91 samples irradiate to 8.3–11.8 dpa.

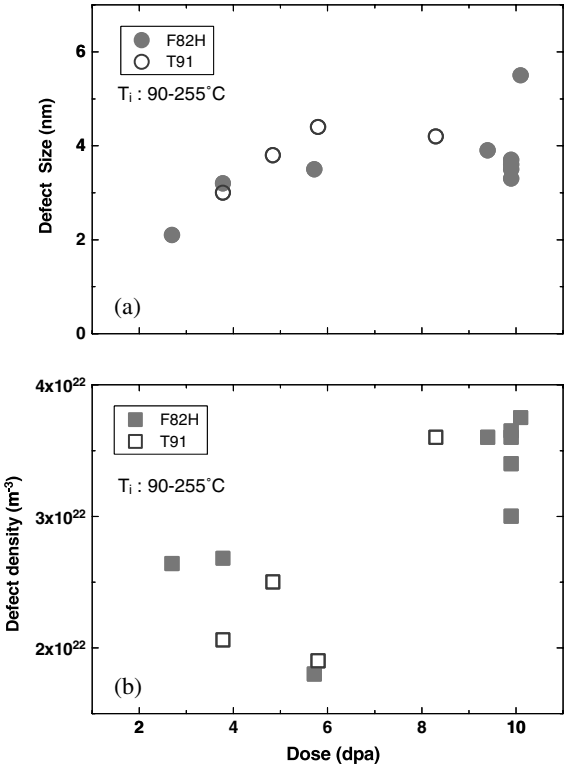

Fig. 5. The dose dependence of the density and the size of defect clusters for F82H and T91 samples irradiated in 90–255 °C.

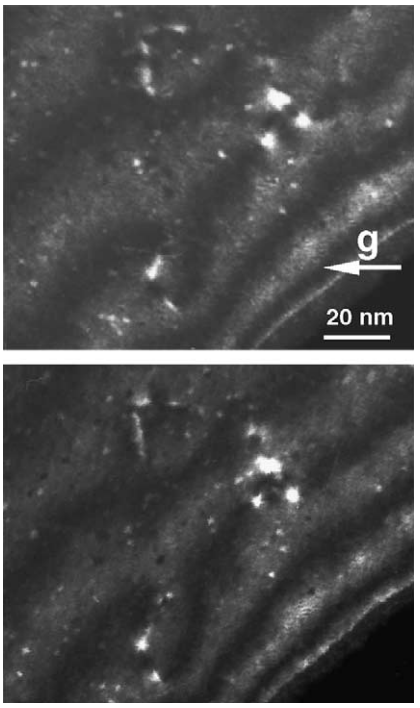

Fig. 6. A stereo pair of WBDF images showing helium bubbles (small white dots) in F82H irradiated to 10.1 dpa at 295 °C. The image condition is **g**(5**g**), **g** = **110**, **z** = **111**.

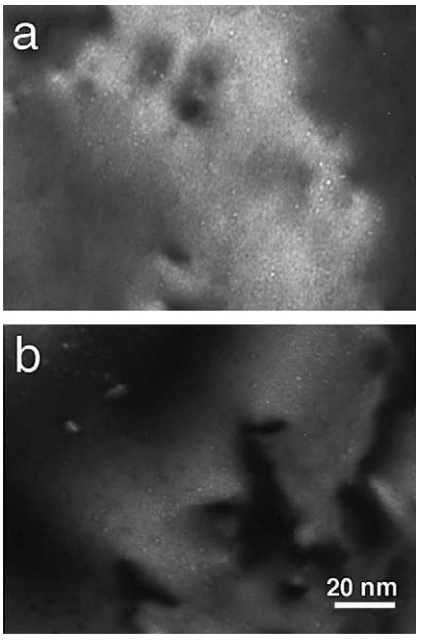

Fig. 7. High-density helium bubbles in (a) F82H irradiated to 9.7 dpa and (b) T91 irradiated to 10.1 dpa at 295 °C.

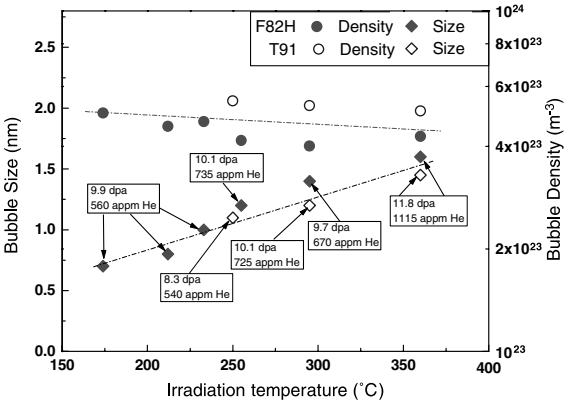

Fig. 8. The temperature dependence of sizes and densities of helium bubbles for T91 and F82H. The irradiation doses and He concentrations are indicated at the size data points.

preferentially at dislocations and grain boundaries. The reason should be the low mobility of helium atoms at low temperatures.

The phenomena of helium bubbles observed in T91 are similar to those in F82H. Fig. 7(a) and (b) demonstrate the bubbles in F82H and T91 irradiated to about 10 dpa at 295 °C, respectively. The quantitative results of the size and density of helium bubble are plotted verse helium concentration in Fig. 8. The bubble size distributions for six samples of F82H and three samples of T91 irradiated at similar conditions are demonstrated in Fig. 9. It can be seen that T91 samples have slightly higher densities but smaller sizes as compared to F82H samples at the same irradiation conditions. For both steels, there are no bubbles can be resolved in the samples irradiated up to 5.8 dpa. As mentioned above that the high-density helium bubbles were observed in F82H steels irradiated at about 175 °C and above in the previous work [6]. No bubbles have been observed in the samples of 5.7 dpa and 375 appm He irradiated at 200 °C. The reason could be that the helium concentration is not high enough. In Table 1 one can see that the helium content in the sample (RC-05) irradiated at 175 °C is 560 appm. Therefore, this indicates that both the helium concentration and the irradiation temperature are important parameters for the formation and growth of helium bubbles. However, the present data are not enough to demonstrate the dose or He concentration dependence of helium bubble size and density. More data from a higher dose range will be obtained soon from the second SINQ target irradiation program.

All the quantitative results of densities and sizes of defect clusters and helium bubbles are presented in Table 1, including those have been published in [6] for a comparison.

Another similar result of the present observation on irradiated T91 is that the $M_{23}C_6$ precipitates become amorphous in the samples irradiated at 110, 130 and

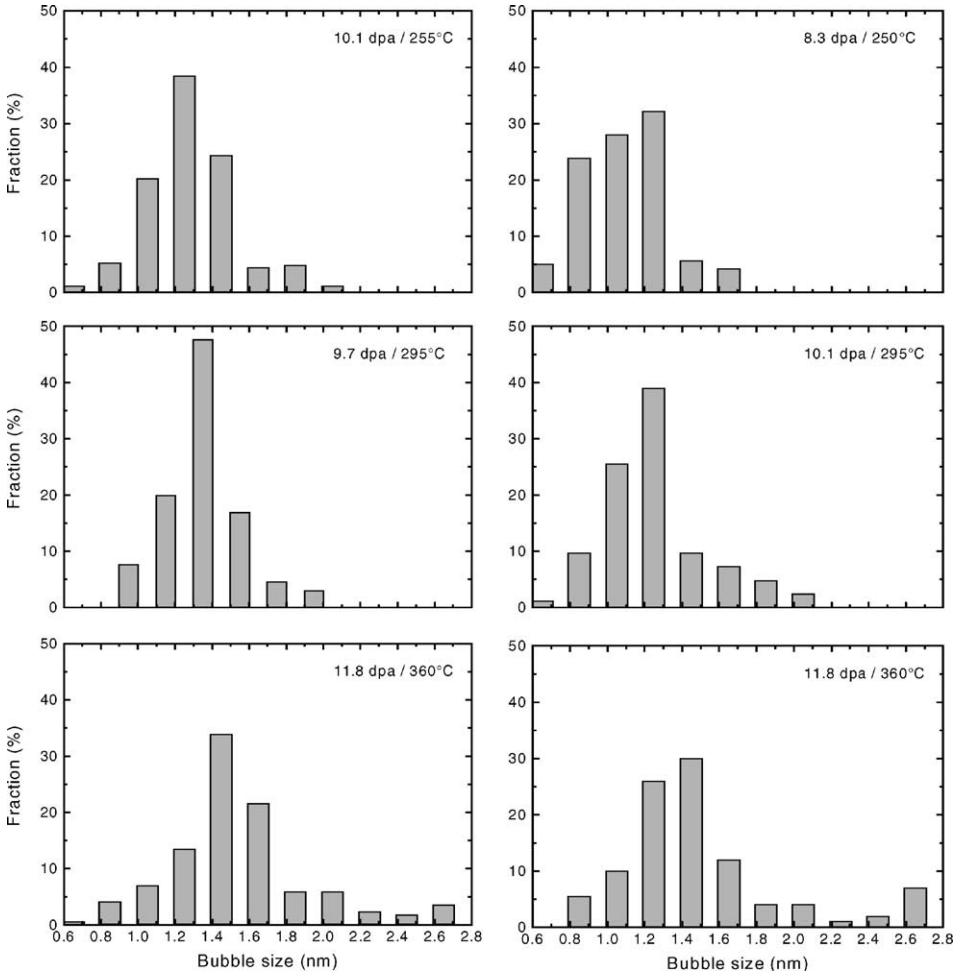

Fig. 9. Bubble size distributions for F82H (left column) and T91 (right column) samples at different irradiation conditions.

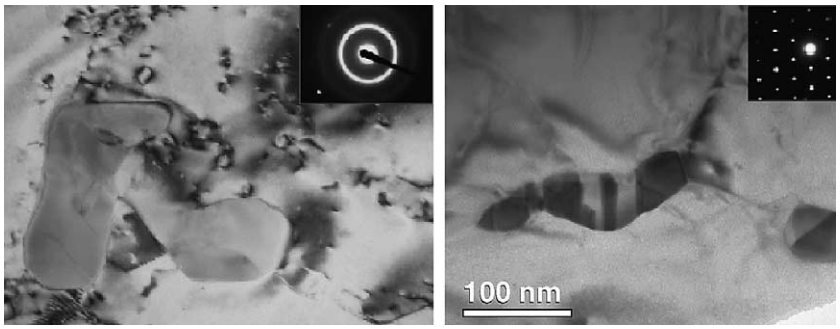

Fig. 10. TEM BF images showing the amorphization of precipitates in T91 steel. left: 5.8 dpa/205 °C, right: 8.3 dpa/250 °C.

205 °C, and remain as crystalline in the samples irradiated at 250, 295 and 360 °C, as shown in Fig. 10 for 205 and 250 °C cases. This is consistent with the previous results of F82H steel, where $M_{23}C_6$ precipitates become amorphous after irradiation at 235 °C and below.

4. Conclusion

TEM discs of martensitic steels F82H and T91 were irradiated in SINQ Target-3 up to 11.8 dpa in a temperature range of 90–360 °C. TEM observations have

been performed to investigate the irradiation effect on the microstructure of both steels. The results show that the microstructure of T91 is very similar to that of F82H at the same conditions, namely:

1. The dislocation and precipitate structures of both steels are similar at the unirradiated condition.
2. After irradiation, the density and size of defect clusters in a T91 sample are almost the same as those in a F82H sample at the same dose. In both steels, the size increases while the density drops rapidly with irradiation temperature above about 250 °C.
3. High-density of helium bubbles of a diameter around 1 nm were observed in both materials when the samples were irradiated to about 10 dpa with about 550 appm He at 175 °C and above. The helium bubbles observed in T91 steel have slightly higher density and smaller size as compared to those in F82H steel irradiated at the same conditions.
4. The amorphization of $M_{23}C_6$ precipitates was observed again in T91 and F82 samples irradiated at $\leqslant 200$ °C, which is consistent with our previous observations.

Acknowledgements

The authors would like to express thanks to Dr K. Farrell for supplying the T91 samples.

This work is included in SPIRE (Irradiation effects in martensitic steels under neutron and proton mixed spectrum) subprogram of the European 5th Framework Program and supported by Swiss Bundesamt für Bildung und Wissenschaft.

References

[1] Y. Dai, G.S. Bauer, F. Carsughi, H. Ullmaier, S.A. Maloy, W.F. Sommer, J. Nucl. Mater. 265 (1999) 203.
[2] Y. Dai, F. Carsughi, W.F. Sommer, G.S. Bauer, H. Ullmaier, J. Nucl. Mater. 276 (2000) 289.
[3] Y. Dai, S.A. Maloy, G.S. Bauer, W.F. Sommer, J. Nucl. Mater. 283–287 (2000) 513.
[4] S.A. Maloy, M.R. James, G. Willcutt, W.F. Sommer, M. Sokolov, L.L. Snead, M.L. Hamilton, F. Garner, J. Nucl. Mater. 296 (2001) 119.
[5] K. Farrell, T.S. Byun, J. Nucl. Mater. 296 (2001) 129.
[6] X. Jia, Y. Dai, M. Victoria, J. Nucl. Mater. 305 (2002) 1.
[7] Y. Dai, X. Jia, K. Farrell, these Proceedings. doi:10.1016/S0022-3115(03)00100-4.
[8] Y. Kohno, D.S. Gelles, A. Kohyama, M. Tamura, A. Hishinuma, J. Nucl. Mater. 191–194 (1992) 868.
[9] Y. Dai, G.S. Bauer, J. Nucl. Mater. 296 (2001) 43.
[10] Y. Dai, Y. Foucher, M.R. James, B.M. Oliver, these Proceedings. doi:10.1016/S0022-3115(03)00099-0.
[11] R. Schaeublin, M. Victoria, J. Nucl. Mater. 283–287 (2000) 339.
[12] J. Henry, M.H. Mathon, P. Jung, these Proceedings. doi:10.1016/S0022-3115(03)00118-1.